Journal of Neuroinflammation

RESEARCH

Open Access

25-hydroxycholesterol promotes brain cytokine production and leukocyte infiltration in a mouse model of lipopolysaccharide-induced neuroinflammation

Johnathan Romero[1], Danira Toral-Rios[1], Jinsheng Yu[2], Steven M. Paul[1,3,4] and Anil G. Cashikar[1,3,4*]

Abstract

Neuroinflammation has been implicated in the pathogenesis of several neurologic and psychiatric disorders. Microglia are key drivers of neuroinflammation and, in response to different inflammatory stimuli, overexpress a proinflammatory signature of genes. Among these, *Ch25h* is a gene overexpressed in brain tissue from Alzheimer's disease as well as various mouse models of neuroinflammation. *Ch25h* encodes cholesterol 25-hydroxylase, an enzyme upregulated in activated microglia under conditions of neuroinflammation, that hydroxylates cholesterol to form 25-hydroxycholesterol (25HC). 25HC can be further metabolized to 7α,25-dihydroxycholesterol, which is a potent chemoattractant of leukocytes. We have previously shown that 25HC increases the production and secretion of the proinflammatory cytokine, IL-1β, by primary mouse microglia treated with lipopolysaccharide (LPS). In the present study, wildtype (*WT*) and *Ch25h*-knockout (*KO*) mice were peripherally administered LPS to induce an inflammatory state in the brain. In LPS-treated *WT* mice, *Ch25h* expression and 25HC levels increased in the brain relative to vehicle-treated *WT* mice. Among LPS-treated *WT* mice, females produced significantly higher levels of 25HC and showed transcriptomic changes reflecting higher levels of cytokine production and leukocyte migration than *WT* male mice. However, females were similar to males among LPS-treated *KO* mice. *Ch25h*-deficiency coincided with decreased microglial activation in response to systemic LPS. Proinflammatory cytokine production and intra-parenchymal infiltration of leukocytes were significantly lower in *KO* compared to *WT* mice. Amounts of IL-1β and IL-6 in the brain strongly correlated with 25HC levels. Our results suggest a proinflammatory role for 25HC in the brain following peripheral administration of LPS.

Keywords Neuroinflammation, 25-hydroxycholesterol, Cholesterol-25-hydroxylase, Lipopolysaccharide, Toll-like receptor-4, Neutrophil infiltration, Cytokines, Microglial activation, Alzheimer's disease

*Correspondence:
Anil G. Cashikar
cashikar@wustl.edu
[1]Department of Psychiatry, Washington University School of Medicine, St Louis, MO 63110, USA
[2]Department of Genetics & Genome Technology Access Center, Washington University School of Medicine, St Louis, MO 63110, USA
[3]Hope Center for Neurological Disorders, Washington University School of Medicine, St Louis, MO 63110, USA
[4]Taylor Family Institute for Innovative Psychiatric Research, Washington University School of Medicine, 425 S Euclid Ave, Campus Box 8134, St Louis, MO 63110, USA

Background

Emerging evidence indicates that neuroinflammation plays an important role in many neurological and psychiatric disorders [1, 2]. Therefore, elucidating the cellular pathways and chemical mediators involved in neuroinflammation could shed light on promising therapeutic targets. Changes in central nervous system (CNS) lipid metabolism, including the synthesis of various cholesterol metabolites, such as bile acids, steroid hormones, and oxysterols, have all been shown to influence immune regulation and neuroinflammation [3]. One oxysterol, 25-hydroxycholesterol (25HC), has especially potent pro- and anti-inflammatory properties under various conditions [4, 5], as well as anti-viral properties against a variety of viruses [6]. 25HC is produced via the enzymatic hydroxylation of cholesterol by cholesterol 25-hydroxylase (CH25H). The *Ch25h* gene is primarily expressed in myeloid cells when challenged with inflammatory stimuli. In the CNS, *Ch25h* is expressed mainly by microglia in mice and humans [7, 8] under inflammatory conditions [9]. Importantly, *Ch25h* is also among a set of genes expressed by disease-associated microglia (DAM) that are chronically upregulated in various neurodegenerative diseases [10, 11]. Taken together, these findings suggest that the principal function of CH25H in the CNS relates to innate immunity and immune surveillance. We and others have postulated that prolonged expression of the enzyme and increased 25HC production may contribute to neuroinflammation and neurodegeneration [12].

The cellular mechanisms by which 25HC regulates immune function appear to stem from its ability to strongly influence cholesterol metabolism, including the suppression of cholesterol biosynthesis and enhancement of cholesterol esterification [13, 14]. Recent studies have provided conflicting evidence about the function of CH25H in modulating inflammation, with some studies reporting greater pro-inflammatory cytokine release [5] and others finding less pro-inflammatory cytokine expression in *Ch25h*-deficient mice [12, 15, 16]. In murine bone-marrow derived macrophages, the SREBP2-SCAP complex, an inhibitory target of 25HC involved in cholesterol metabolism, was found to facilitate inflammasome activation, suggesting an anti-inflammatory role for CH25H [17]. However, in murine brain-resident macrophages (i.e., microglia), 25HC increased interleukin-1-beta (IL-1β) secretion, indicating a potential pro-inflammatory role for CH25H in the CNS [12]. Known potent inducers of *Ch25h* expression include ligands of type I interferon receptors (IFNRs) and Toll-like receptors (TLRs), particularly TLR4 [18]. Lipopolysaccharide (LPS), a surface glycolipid found in most Gram-negative bacteria, is a TLR4 agonist that not only increases *Ch25h* expression [18], but also acutely alters the synthesis of several lipids, most notably phosphatidylethanolamine and docosatetraenoic acid, in the mouse brain [19]. Similarly, treatment of immortalized murine microglia with LPS has also been shown to increase diacylglycerols and triacylglycerol [20] synthesis. Moreover, LPS triggers many of the inflammatory processes involved in neurodegeneration, including cytokine release, gliosis, and peripheral leukocyte infiltration. Recently, neuroinflammation has been extensively studied in the context of mouse models of neurodegeneration and demyelination [21, 22]. Peripheral injection of LPS can model neuroinflammation by acutely inducing neuroinflammation that mimics bacterial infection [23].

To better understand the role of CH25H and 25HC in neuroinflammation, we administered LPS peripherally to induce neuroinflammation in *Ch25h* knockout and wildtype female and male mice. Our results also indicate that in a mouse model of LPS-induced neuroinflammation, while higher 25HC levels in wildtype mice correlate with increased proinflammatory responses, loss of *Ch25h* gene reduces it.

Results

Intraperitoneal administration of LPS induces *Ch25h* expression and 25HC synthesis in the brain

To understand how *Ch25h* and 25HC influence neuroinflammation, we intraperitoneally (i.p) administered LPS or vehicle (PBS) twice (two-hit LPS model) in wildtype (*WT*) and *ch25h-/-* (*KO*) mice (Fig. 1A). This LPS-mediated neuroinflammation model was recently shown to result in increased cytokine levels as well as neutrophil infiltration in the brain [24]. Expression of *Ch25h* was confirmed in the *WT* and *KO* cohorts by qPCR. Replicating findings from previous studies [18, 25, 26], LPS administration promoted the upregulation of *Ch25h* expression in *WT* mice by almost 10-fold ($p<0.0001$) and, as expected, no expression in the *KO* group was observed (Fig. 1B). Based on single-cell transcriptomics studies [7, 8, 27] it is likely that *Ch25h* overexpression is mainly due to activated microglia (also see The Myeloid Landscape 2).

To confirm that the increase in *Ch25h* expression resulted in an increase in 25HC synthesis, the relative concentrations of 25HC (normalized to tissue weight) was quantified in the cortical tissue by liquid chromatography/mass spectrometry (LC/MS) (Fig. 1C). Consistent with the expression of *Ch25h*, a significant increase ($p<0.0001$) in the relative amounts of 25HC was observed in the LPS-treated *WT* compared to the PBS-treated *WT* mice, while the *KO* cohort demonstrated levels of 25HC that were lower or comparable to the PBS control. The low levels of 25HC observed in brain tissue from PBS-treated *WT* mice and in *KO* mice are presumably produced by pathways independent of CH25H enzyme activity such as cholesterol hydroxylation by

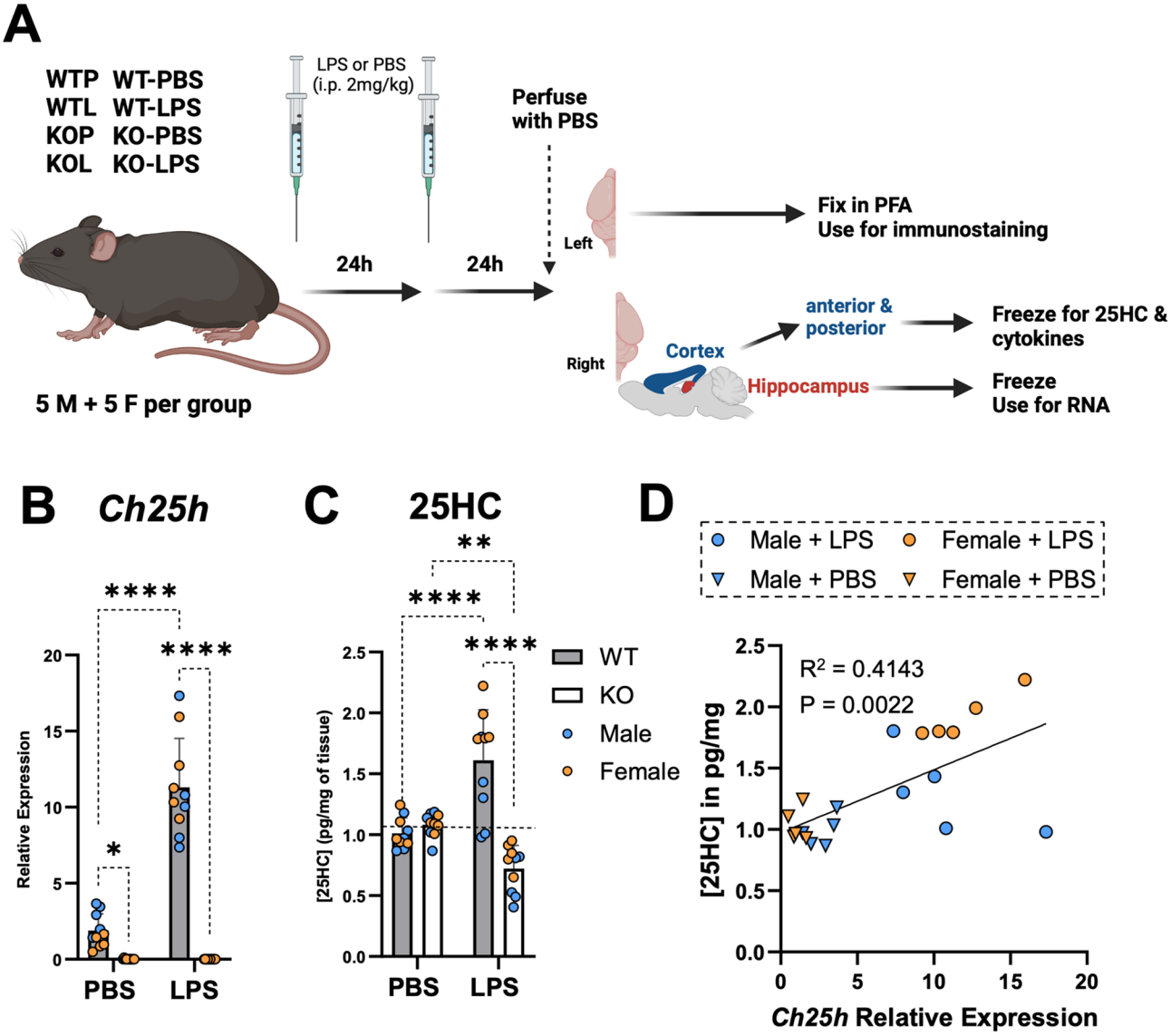

Fig. 1 Mouse model for LPS-mediated neuroinflammation and quantification of 25HC and *Ch25h* expression. (**A**) Schematic of 2-hit LPS mouse model. (**B**) Relative expression of *Ch25h* and (**C**) measured concentrations of 25HC in PBS- and LPS-injected wildtype (*WT*) and *Ch25h*-deficient (*KO*) mouse brains. Male mice are indicated in blue and female mice are in orange. Data are presented as mean values ± SD ($n = 5$ per sex per genotype per treatment group). Statistical significance was defined using a two-way ANOVA with Fisher's LSD post-hoc multiple comparisons test (*$P < 0.05$, **$P < 0.01$, & ****$P < 0.0001$). Gene expression was normalized with b-actin. (**D**) Correlation plot of *Ch25h* mRNA expression and 25HC produced in the brain tissue. Male mice are indicated in blue and female mice are in orange; PBS controls are inverted triangles and LPS-treated mice are circles – as shown at the top of the correlation plot. All points were fit by linear regression and the R^2 and P values are shown at the top left

CYP3A4, as reported earlier [28]. Increased production of 25HC in LPS-treated samples correlates with *Ch25h* mRNA expression (R^2=0.414, p=0.0022) (Fig. 1D) indicating that the 25HC synthesized after LPS-treatment resulted from CH25H enzyme activity. To ensure that changes in structurally isomeric oxysterols did not skew the 25HC measurements, we also determined the concentrations of the two isomeric oxysterols – namely, 24 S-hydroxycholesterol (24(S)HC) and 27-hydroxycholesterol (27HC) – that are appreciably present in the CNS (Fig. S1A & B). Confirming that LPS selectively induces 25HC synthesis, treatment with LPS did not increase levels of 24(S)HC or 27HC. Thus, we conclude that peripheral administration of LPS induces the expression of *Ch25h* in the brain, leading to elevated 25HC synthesis.

Interestingly, LPS-induced 25HC synthesis in female *WT* mice appeared to be higher than in male *WT* mice (n=5 per sex per genotype per treatment group), but higher sample sizes are necessary to confirm this finding. Since no significant difference was evident between males and females in the expression of *Ch25h* mRNA, we tested whether 7α-hydroxylation of 25HC accounts

for the difference between males and females by examining the expression of *Cyp7b1*, the gene encoding the enzyme for 7α-hydroxylation of 25HC to produce 7α,25-dihydroxycholesterol. No significant differences in *Cyp7b1* expression related to LPS treatment were apparent in *WT* mice (Fig. S2), suggesting that other unknown metabolic pathways may be involved in determining 25HC levels.

Ch25h deficiency reduces gliosis induced by LPS administration

Activation of brain-resident immune cells (i.e., microglia) is associated with neuroinflammation. To assess the role of CH25H in promoting microglial activation, hippocampal sections of wildtype and *Ch25h*-deficient mice were probed for markers of microglial activation by immunostaining for ionized calcium-binding adaptor molecule 1 (IBA1, Fig. 2A) as well as the microglial phagocytosis marker cluster of differentiation 68 (CD68, Fig. 2C), expressed by activated microglia. As a discrete, easily identifiable brain structure that facilitates quantitation and mitigates variability across brains, the hippocampus was chosen for immunohistochemical analysis. In another study with the *Ch25h*-deficient mice in the PS19 tau transgenic model of tauopathy, we showed strong reductions in neuroinflammation and neurodegeneration in the hippocampus [29]. Furthermore, LPS-induced neuroinflammation displayed no obvious region-specificity in the brain. As expected, LPS treatment significantly increased the area covered by IBA1 ($p<0.001$, Fig. 2B) and CD68 ($p<0.0001$, Fig. 2D) immunoreactivity in *WT* mice compared with the PBS-treated *WT* mice, while no significant effect of *Ch25h* genotype on IBA1 immunoreactivity was observed (Fig. 2A & B). However, CD68 immunoreactivity was substantially lower ($p<0.0001$) in *Ch25h*-deficient mouse hippocampi, suggesting that microglial activation is elevated by *Ch25h* (Fig. 2C & D). Additionally, while levels of CD68 and IBA1 appeared to form distinct clusters by sex in the LPS-treated *KO* and *WT* cohorts, larger sample sizes per group are required to ascertain these results.

To investigate additional markers of microglial activation, we quantified the relative expression of markers of disease-associated microglia (DAM) (Fig. 2E-G) – namely, *Trem2* (triggering receptor expressed on myeloid cells 2), *Clec7a* (C-type lectin domain family member 7 A), and *Axl* (tyrosine-protein kinase receptor UFO). An LPS-dependent change in *Trem2* expression was observed in *KO*, but not *WT* samples and expression of *Trem2* mRNA was significantly lower ($p<0.01$) in the *KO* samples among the LPS-treated cohort (Fig. 2E). With LPS treatment, *Clec7a* expression was significantly higher in LPS-treated *WT* compared to *KO* mice ($p<0.01$) and PBS-control *WT* mice ($p<0.01$) (Fig. 2F). LPS-dependent upregulation ($p<0.0001$) of *Axl* mRNA was also observed in the *WT* mice but not in *KO* mice (Fig. 2G). These results suggest that despite similar IBA1 immunoreactivity between *WT* and *KO* mice, microglial activation was significantly lower in *Ch25h*-deficient mice.

Serial systemic or local injections of LPS in mice have been shown to induce astrogliosis. Accumulating evidence indicates that altered lipid metabolism is associated with reactive astrogliosis [30, 31]. We recently reported that 25HC markedly suppresses cholesterol biosynthesis and increases cholesterol esterification as well as cholesterol efflux via ApoE lipoproteins in murine primary astrocytes [14] and suggests a possible role for 25HC in astroglial activation. Therefore, to evaluate how 25HC influences astrogliosis in vivo, we immunostained mouse brain sections for glial fibrillary acidic protein (GFAP) (Fig. 3A). Quantitation of the immunostained images showed a significant increase ($p<0.05$) in the percent area of GFAP immunoreactivity in the hippocampi of LPS-treated *WT* mice compared with the PBS-injected mice. Interestingly, among the LPS-injected mice, significantly less area of GFAP immunoreactivity ($p<0.01$) was observed in the *KO* cohort (Fig. 3B). No differences were detected between *WT* and *KO* mice treated with PBS. To corroborate these findings on the effect of 25HC in astrogliosis, the relative expression of *Gfap* was quantified in the hippocampus by qPCR. In agreement with the results from the immunofluorescence staining, the relative expression of *Gfap* mRNA increased ($p<0.0001$) by 2-3-fold in the LPS-treated mice compared to PBS-treated mice (Fig. 3C). Although *Gfap* expression in LPS-treated *KO* mice was slightly lower than *WT* mice, the difference was not significant (Fig. 3C). Additionally, GFAP levels showed no differences between the sexes in protein or mRNA levels, although further experiments with larger sex-specific cohorts are necessary to confidently corroborate these findings.

Ch25h deficiency differentially influences LPS-mediated transcriptomic changes in males and females

To understand the underlying mechanisms by which CH25H and 25HC may influence neuroinflammation in this mouse model of LPS-induced neuroinflammation, we carried out transcriptome analysis (bulk tissue RNA-seq) of the hippocampus. Gene expression in this study is potentially affected by three different variables – namely, treatment (LPS vs. PBS), genotype (*KO* vs. *WT*), and sex (females vs. males).

Treatment with LPS resulted in major transcriptomic changes in both a genotype- and sex-dependent manner (Supp. Table I). While LPS treatment resulted in a greater number of differentially expressed genes in females, *Ch25h* deficiency resulted in fewer gene expression changes in the brains of female mice. When

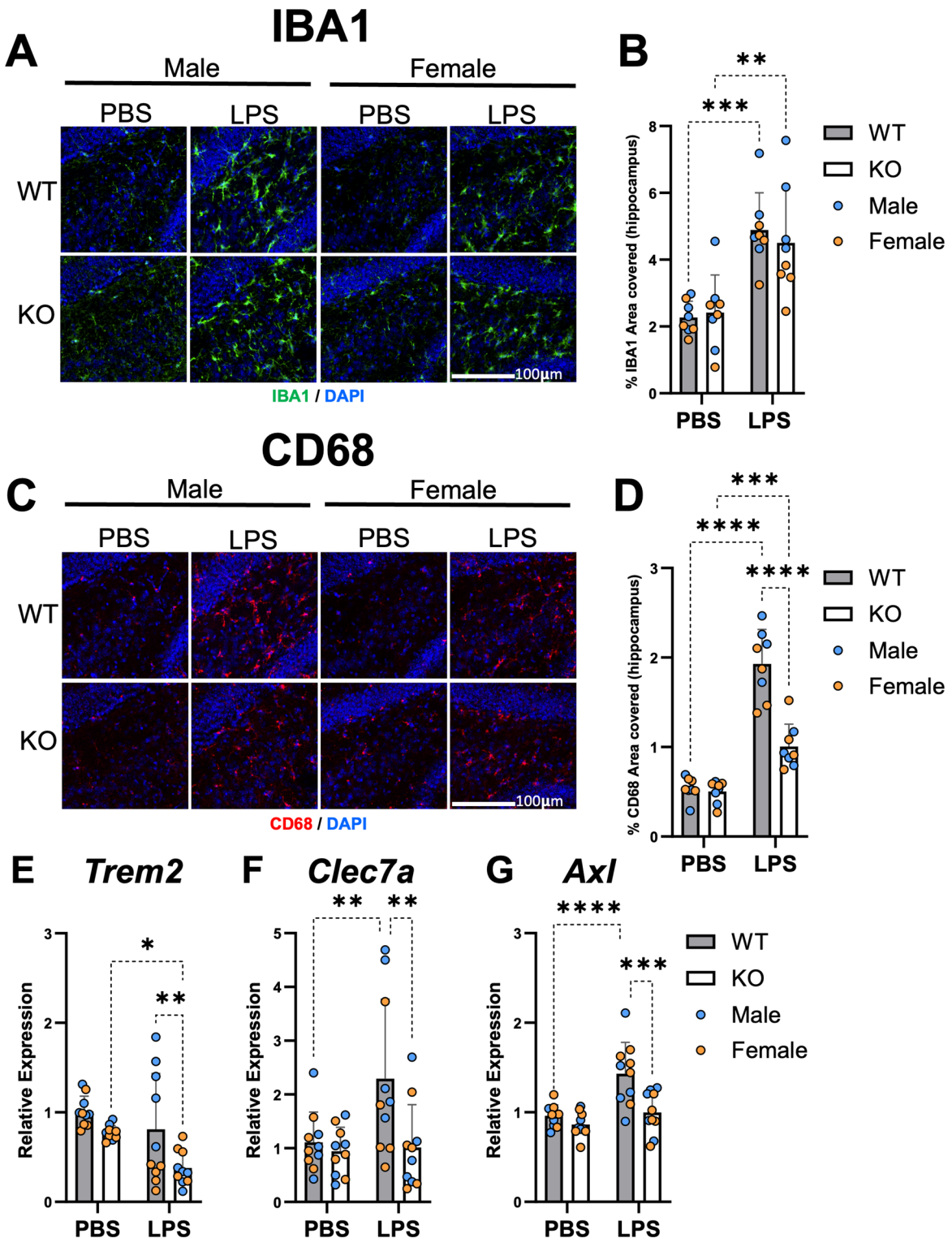

Fig. 2 Microglial activation triggered by LPS treatment was mitigated by loss of *Ch25h*. Representative images of immunostaining (**A**) and quantification (**B**) by percentage of IBA1 area in the dentate gyrus. Representative images of immunostaining (**C**) and quantification (**D**) by percentage of CD68 area in the dentate gyrus. Data are presented as mean values ± SD ($n = 4$ per sex per genotype per treatment group). Relative expression of *Trem2* (**E**) *Clec7a* (**F**) and *Axl* (**G**). Gene expression was normalized with b-actin. Male mice are indicated in blue, and female mice are in orange. Data are presented as mean values ± SD ($n = 5$ per sex per genotype per treatment group). Statistical significance was defined using a two-way ANOVA with Fisher's LSD post-hoc test (*$P < 0.05$, **$P < 0.01$, ***$P < 0.001$, & ****$P < 0.0001$)

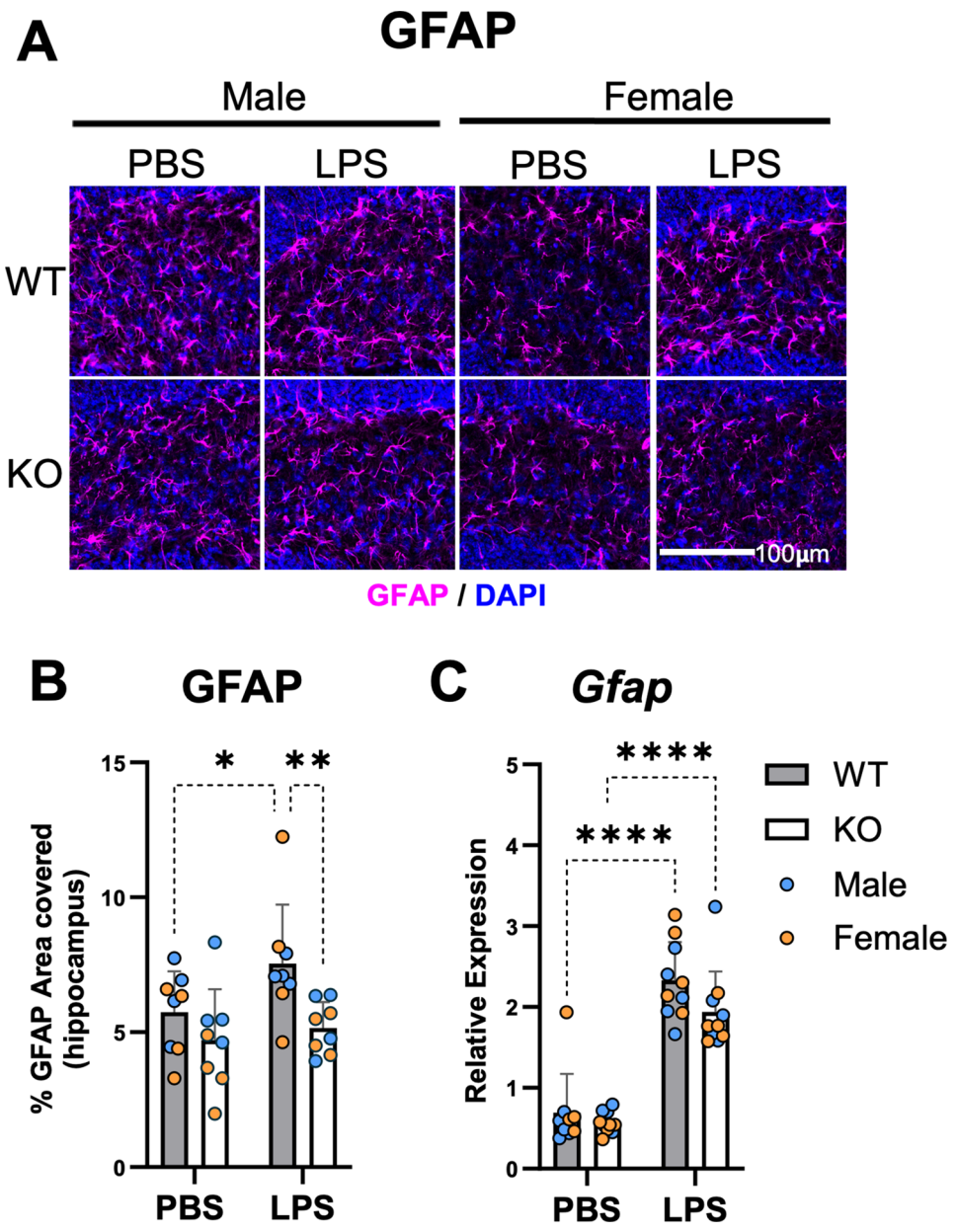

Fig. 3 LPS-induced astrogliosis. Representative images of immunostaining (**A**) and quantification (**B**) by percentage of GFAP area in the dentate gyrus. Data are presented as mean values ± SD ($n = 4$ per sex per genotype per treatment group). (**C**) Relative expression of *Gfap* mRNA. Male mice are indicated in blue, and female mice are in orange. Data are presented as mean values ± SD ($n = 5$ per sex per genotype per treatment group). Statistical significance was defined using a two-way ANOVA with Fisher's LSD post-hoc multiple comparisons test (*$P < 0.05$, **$P < 0.01$, & ****$P < 0.0001$)

differential gene expression between females and males was examined (Supp. table II), female *WT* mice showed greater differential gene expression in response to LPS treatment than male *WT* mice (158 genes up and 66 genes down for fold change > 1.5 and q < 0.05). Interestingly, such sex-specific differences in the response to LPS were not apparent in *KO* mice (3 genes up and 4 genes down for fold change > 1.5 and q < 0.05). The differentially expressed genes in response to LPS treatment are shown as volcano plots in Figure S3. Complete lists of differentially expressed genes (DEGs) in response to LPS (LPS vs. PBS) in each group are listed in Supplementary Table I and the corresponding gene ontology (GO) terms are shown in Figure S4. The differentially upregulated genes following LPS treatment were grouped into GO terms: 'regulation of defense response', 'regulation of cytokine production', 'leukocyte migration,' and others (Fig. 4A).

To understand whether sex played a role in LPS-mediated neuroinflammation in mice, we compared the LPS response of female and male *WT* and *KO* mice side-by-side (Fig. 4A and Supp. Table III). Comparisons of the upregulated pathways in response to LPS treatment

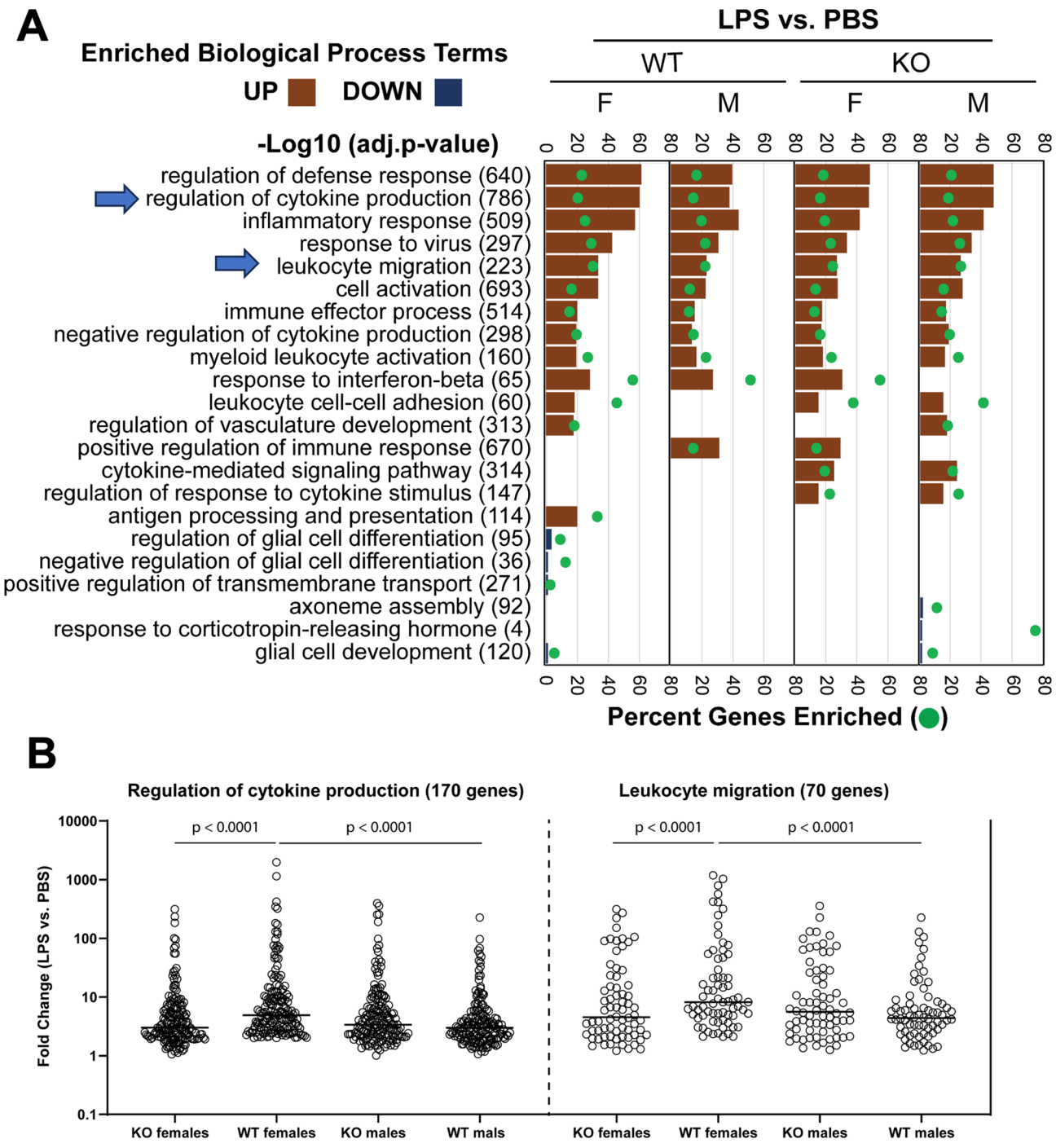

Fig. 4 Transcriptomics of mouse hippocampi. (**A**) Comparison of the LPS effect on female (F) and male (M) mice in the wildtype (*WT*) and *Ch25h* knockout (*KO*) groups ($n = 5$ per sex per genotype per treatment group). The horizontal brown bars under each group show -log10 (adj. P value) for the gene ontology (GO) biological process on the top X-axis. The green circle shows the percent of genes enriched within each GO term. (**B**) Wilcoxon paired test to compare transcriptomic changes in WT female mice relative to WT male mice and KO female mice in 170 genes in the 'cytokine production' GO group (left) and 70 genes in the 'leukocyte migration' GO group (right). As the Fold change data did not pass a normality test, median values are indicated with a horizontal line for each group. The relevant data and details of the Wilcoxon test are available in Supp. Table IV

(Supp. Table IV) revealed that – (i) cytokine production genes included 21.6% hits (log10 q value = -61.48) in *WT* females; 15.5% hits (log10 q value = -38.28) in *WT* males; 17.04% hits (log10 q value = -48.16) in *KO* females; and 19.2% hits (log10 q value = -48.18) in *KO* males. (ii) leukocyte migration genes included 31.4% hits (log10 q value = -34.45) in *WT* females; 23.31% hits (log10 q value = -23.24) in *WT* males; 25.11% hits (log10 q value

= -27.33) in *KO* females; and 27.35% hits (log10 q value = -26.6) in *KO* males. We also carried out Wilcoxon paired tests to determine whether *WT* female mice significantly differed from *WT* male mice and *KO* female mice (Fig. 4B and Supp. Table IV). For this test, we compared the 170 upregulated genes the 'cytokine production' GO group and the 70 upregulated genes in the 'leukocyte migration' GO group. These comparisons with the Wilcoxon tests reveal that LPS treatment triggered significantly greater expression of genes involved in cytokine production and leukocyte migration in *WT* females relative to *WT* males or *KO* females (Fig. 4B and Supp. Table IV). Comparisons of the downregulated genes and pathways in response to LPS treatment (Supp. Table IV) revealed that regulation of glial differentiation genes included 10.52% hits (log10 q value −3.83) only in *WT* females and no other groups. Furthermore, sex had little impact on the LPS response (up- or down-regulated genes) in *KO* mice – that is, female and male KO mice responded similarly to LPS.

Taken together, these results suggest *WT* female mice had a stronger neuroinflammatory response to LPS than *WT* male mice and that these sex-dependent differences in gene expression were absent in *Ch25h*-deficient mice. To further understand this effect, we focused on how *Ch25h*/25HC influences cytokine production and leukocyte migration into the brain parenchyma.

25HC concentrations correlate with cytokine levels

To ascertain the effects of *Ch25h* deficiency on pro-inflammatory cytokine production and gene transcription, we also measured gene expression and secreted cytokine levels for interleukin 1 beta (*Il1b* and IL-1β; Fig. 5A, B & C), tumor necrosis factor-alpha (*Tnf* and TNF; Fig. 5D, E & F), and interleukin 6 (*Il6* and IL-6; Fig. 5G, H & I) by qPCR and ELISA, respectively. LPS treatment resulted in a substantial upregulation of these cytokine mRNAs in both *WT* and *KO* samples. Expression of *Il1b* increased by nearly 50-fold in LPS-treated *WT* brains relative to PBS-treated controls ($p<0.0001$). Furthermore, *Il1b* expression was significantly lower ($p<0.05$) in LPS-treated *KO* samples (Fig. 5A), which is consistent with our earlier report on *WT* and *KO* microglia studied in vitro [12]. Measurement of IL-1β protein levels in brain extracts corroborated the mRNA findings (Fig. 5B). Moreover, the brain levels of IL-1β showed a striking correlation with the levels of 25HC (from Fig. 1C) ($R^2=0.607$; $p<0.0001$) (Fig. 5C). LPS-treated female mice that produced higher brain levels of 25HC also largely had higher brain levels of IL-1β relative to male mice.

Although expression of *Tnf* mRNA also significantly increased with LPS treatment ($p<0.01$) (Fig. 5D) in *WT* mice, this was not reflected by protein levels (Fig. 5E). *Ch25h* deficiency did not influence *Tnf* mRNA expression or TNF protein levels in the brain. 25HC levels did not correlate ($R^2=0.1871$, $p<0.0644$) with TNF protein levels (Fig. 5F).

LPS treatment promoted significant ($p<0.05$) increases in IL-6 protein levels and mRNA expression in *WT* and *KO* mice (Fig. 5G & H). In addition, significantly lower levels of IL-6 protein were observed in *KO* samples relative to *WT* after LPS treatment and 25HC levels correlated moderately with IL-6 protein levels (Fig. 5I, $R^2=0.4446$, $p<0.0018$).

These observations show that *Ch25h*-deficient mice present a reduced proinflammatory cytokine profile (especially for IL-1β), as predicted by the transcriptomic results.

CH25H promotes leukocyte infiltration into the brain induced by LPS

Recent work using this experimental paradigm has shown that 2-hit systemic LPS administration is sufficient to stimulate infiltration of leukocytes into the brain parenchyma [24]. We previously observed decreased expression levels of *Cxcl10* in *Ch25h*-deficient mouse primary microglia treated with tau fibrils [29], a key interferon-gamma-inducible chemokine that may facilitate leukocyte infiltration into the brain [32]. A closer examination of the DEGs in the 'leukocyte migration' GO group from the RNAseq data (Fig. 4, Supp. Tables I, III and IV) revealed that *Cxcl10* expression is significantly higher in *WT* female mice relative to *WT* male mice or *KO* female mice. Other chemokines that may also play a role in leukocyte chemotaxis such as *Ccl2*, *Ccl3* and *Ccl4* were also higher in *WT* female mice relative *WT* male mice or *KO* female mice. To test whether *Ch25h* expression may promote leukocyte recruitment into the brain induced by LPS, a single cell suspension was isolated from the right hippocampi and cortices of mice (Fig. 6A). Populations of T lymphocytes ($CD45^{hi}Cd11b^{-}TCRb^{+}$), Natural killer (NK) cells ($CD45^{hi}Cd11b^{-}TCRb^{-}NK1.1^{+}$), Natural killer T (NKT) cells ($CD45^{hi}Cd11b^{-}TCRb^{+}NK1.1^{+}$) and Neutrophils ($CD45^{hi}Cd11b^{+}LY6G^{+}$) were identified and analyzed by flow cytometry (Fig. 6B).

Administration of LPS led to a dramatic increase (~30 fold-change, $p<0.0001$) in the proportion of neutrophils ($CD45^{hi}Cd11b^{+}LY6G^{+}$) in the brain compared with PBS-treated controls (Fig. 6C). A trend towards decreased proportion of neutrophils in LPS-treated *KO* mice was observed relative to *WT* mice, but it was not significant ($p=0.0662$). To ascertain the potential role of CH25H in the LPS-induced CNS infiltration of neutrophils, we examined the presence of the neutrophil-specific marker lymphocyte antigen 6 complex locus G6D (LY6G) using qPCR (Fig. S5A & B) and by immunostaining (Fig. S5C & D). *Ly6g* mRNA levels increased about 50-100-fold following LPS treatment in *WT* mouse brain. This

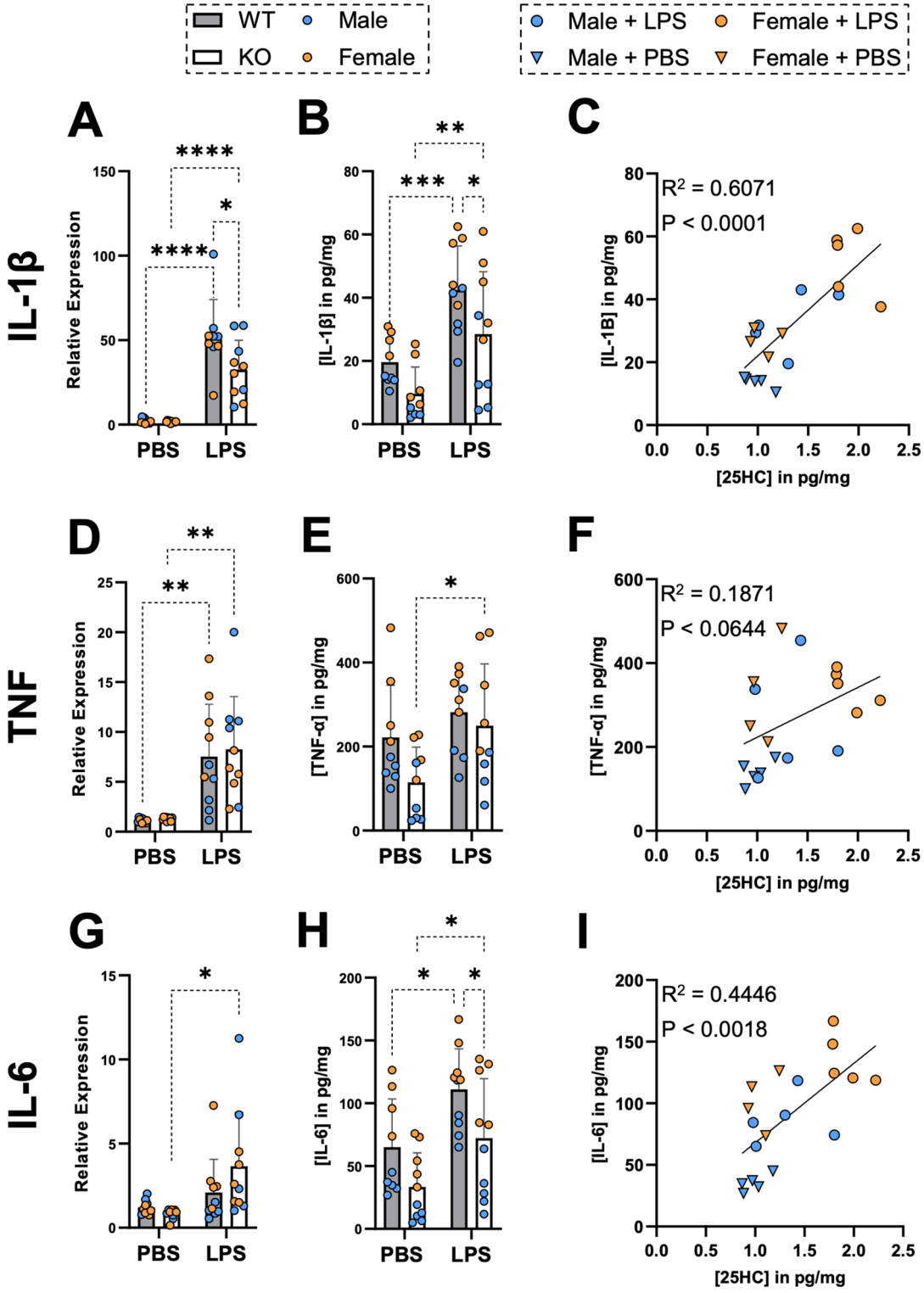

Fig. 5 Levels of 25HC correlate with cytokine protein and gene expression. Relative expression of *Il1b* (**A**), *Tnf* (**D**) and *Il6* (**G**) mRNA in hippocampus. Concentrations of IL-1β (**B**), TNF (**E**), and IL-6 (**H**) determined by ELISA and their respective correlations (**C**, **F** & **I**) with 25HC levels. 25HC concentrations are as shown in Fig. 1C. Male mice are indicated in blue, and female mice are in orange. PBS controls are inverted triangles and LPS-treated mice are circles as shown at the top of the correlation plot. Data are presented as mean values ± SD ($n = 5$ per sex per genotype per treatment group). Statistical significance was defined using a two-way ANOVA with Fisher's LSD post-hoc test (*$P < 0.05$, **$P < 0.01$, ***$P < 0.001$, & ****$P < 0.0001$). Statistical significance and slope of the line were calculated with simple linear regression analysis and correlations were assessed by calculating the coefficient of determination (R^2)

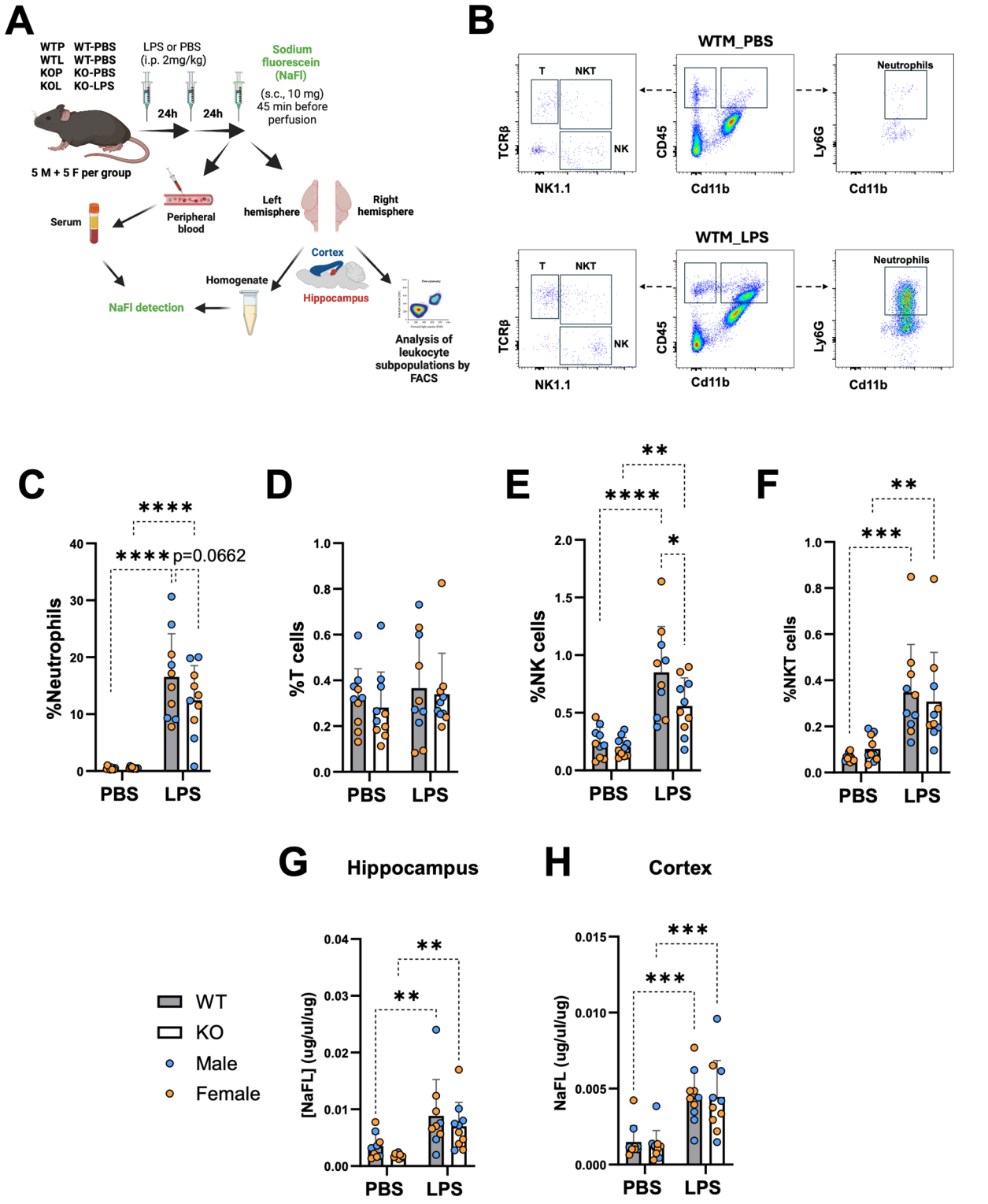

Fig. 6 Role of CH25H/25HC in brain leukocyte infiltration mediated by LPS administration. (**A**) Schematic of the experimental design to assess BBB permeability using sodium fluorescein (NaFl) and leukocyte infiltration using flow cytometry in the 2-hit LPS model in wildtype (*WT*) and Ch25h-deficient (*KO*) mouse. (**B**) Flow cytometry gating strategy and representative flow cytometry plots showing neutrophils ($CD45^{hi}Cd11b^{+}LY6G^{+}$), T cells ($CD45^{hi}Cd11b^{-}TCRB^{+}$), NK cells ($CD45^{hi}Cd11b^{-}TCRB\text{-}NK1.1^{+}$) and NKT cells ($CD45^{hi}Cd11b^{-}TCRB^{+}NK1.1^{+}$). Percentage of neutrophils (**C**), T cells (**D**), NK cells (**E**) and NKT cells (**F**) relative to total single cells in mouse brain tissues. Quantification of NaFl in hippocampus (**G**) and cortex (**H**) of PBS- and LPS-injected *WT* and *KO* mice. Male mice are indicated in blue, and female mice are in orange. Data are presented as mean values ± SD ($n = 5$ per sex per genotype per treatment group). Statistical significance was defined using a two-way ANOVA with Fisher's LSD post-hoc multiple comparisons test (*$P < 0.05$, **$P < 0.01$, ***$P < 0.001$, & ****$P < 0.0001$)

increase was significantly reduced ($p<0.01$) in the *KO* mice (Fig. S5A). Importantly, the brain concentrations of 25HC in *WT* mice (Fig. 1C) showed a striking correlation ($R^2=0.696$, $p<0.0001$) with relative expression of *Ly6g* mRNA (Fig. S5B). suggesting that neutrophil infiltration might be promoted by 25HC synthesized from CH25H. To corroborate if the increase in *Ly6g* mRNA was reflected by an increase in $LY6G^+$ neutrophils in the brain parenchyma, we immunostained mouse brain tissue sections with an antibody specific to mouse LY6G (Fig. S5C) and observed a significant increase ($p<0.01$) in the percentage of area covered by LY6G immunoreactivity only in LPS-treated *WT* mice but not in *KO* mice (Fig. S5D).

In contrast to previous observations of T-cell infiltration into the brain observed in the 2-hit systemic LPS administration model [24], the proportion of T cells ($CD45^{hi}TCRb^+$) in the brain did not change following LPS administration (Fig. 6D). Similar results were observed when we analyzed immunoreactivity for the T-cell receptor CD3 in the hippocampi of mice from our first cohort injected with LPS (Fig. S5E).

LPS administration led to a significant increase in the proportion of NK cells (~3.5 fold change, $p<0.0001$) and NKT cells (~5.3 fold change, $p<0.001$) relative to mice injected with PBS (Fig. 6E and F). Genetic ablation of *Ch25h* resulted in a reduction (~30% change, $p<0.05$) in the recruitment of NK cells into the brain mediated by LPS (Fig. 6E). However, *Ch25h* deficiency did not alter the proportion of NKT cells relative to *WT* mice (Fig. 6F). Taken together, our results indicate that *Ch25h* expression promotes the infiltration of NK cells and likely neutrophils into the brain following systemic LPS administration.

Ch25h deficiency does not alter blood-brain barrier permeability

An increase in the permeability of the blood-brain barrier (BBB) induced by LPS exposure may explain this influx of leukocytes. Previous studies indicate that systemic LPS challenge increases BBB permeability [33, 34] that can result in extravasation of blood products, cytokines, and perhaps LPS itself, which may explain the neuroinflammatory effect of peripherally circulating LPS. Therefore, the role of CH25H/25HC on LPS-induced BBB permeability was assessed by injection of fluorescein sodium salt (NaFl) [35] in a second cohort of genotype-, sex-, and age-matched mice that previously received either two injections of LPS or PBS (Fig. 6A). After intracardial perfusion and tissue harvesting, the left hippocampi and anterior cortices were collected for fluorescence estimation of NaFl. Serum was also extracted to control for circulating levels of dye in the blood and fluorescence measurements were normalized to tissue weight. LPS treatment was associated with a significant increase in NaFl in hippocampi ($P<0.001$; Fig. 6G) and anterior cortices ($P<0.001$; Fig. 6H). However, no effect of *Ch25h* genotype on fluorescence was observed. Therefore, our findings replicate those of previous studies [33, 34, 36] showing that LPS increases BBB permeability and demonstrate that CH25H expression does not alter BBB permeability in this model.

Discussion

In this study, we use the "two-hit" model of intraperitoneal LPS administration [24] to investigate the role of CH25H/25HC in LPS-induced neuroinflammation.

A growing body of research implicates neuroinflammation in the pathogenesis and progression of neurodegenerative disorders, such as AD [36, 37], with accumulating evidence suggesting roles for both innate and adaptive immunity [38–42]. There is also evidence that bacterial [43, 44] and viral [45, 46] infections as well as alterations in the microbiome [47] may contribute to disease pathogenesis. Neuroinflammation often results when a peripheral infection spreads to the CNS. Activation of pattern-recognition receptors (PRRs) by pathogen-associated molecular patterns (PAMPs) occurs early in the brain's innate immune response to detect invading pathogens and initiate an inflammatory response. One class of PRRs, the Toll-like receptors (TLRs), are crucial for the innate immune response to bacterial infection. Toll-like receptor 4 (TLR4) canonically binds to the near-ubiquitously expressed Gram-negative bacterial cell-surface antigen, LPS, and is an important early trigger of inflammation in response to Gram-negative bacterial infection. TLR4 inhibition or impairment has been shown to reduce brain inflammation in mouse models and influence the pathophysiology of neurodegenerative disease [48–50]. Recent work has found that periodontitis caused by bacterial infection of the gingiva is associated with an increased risk of AD [51], suggesting that certain bacterial infections may increase the risk of developing AD. Given the prevalence of Gram-negative bacteria in periodontitis and its proximity to cerebral blood vasculature, the circulation of Gram-negative bacteria (or LPS) near the blood-brain barrier is plausible. In the mouse model of neuroinflammation employed in our study, even peripheral LPS administration is sufficient to induce TLR4-mediated inflammation in brain parenchyma. Remarkably, even a single peripheral administration of LPS in wild-type mice has been reported to result in neuroinflammation that persists over an entire year [23], suggesting similar mechanisms may prolong the inflammatory state in the human CNS.

Cholesterol 25-hydroxylase (*Ch25h*) is markedly upregulated by LPS treatment and is one of the genes expressed by disease-associated microglia (DAM) that

are chronically upregulated in various neurodegenerative disorders [10, 11]. Prolonged expression of *Ch25h* and 25HC production may contribute to neuroinflammation and consequent neurodegeneration. In fact, we have recently observed that *Ch25h*/25HC deficiency markedly reduces the age-dependent neuroinflammation and neurodegeneration observed in the P301S tau transgenic mice [29].

Reinforcing the findings from our immunochemical and qPCR assays, RNA-seq analysis of mouse hippocampal samples found that LPS significantly increased transcription associated with immune-related biological pathways related to cytokine production, anti-viral immune response, immune cell activation, leukocyte infiltration, and inflammation more broadly (Fig. 4).

While LPS treatment led to a significant increase in the immunoreactivity of the microglial maker, IBA1, in the hippocampus of both *WT* and *KO* mice, *Ch25h* deficiency did not affect IBA1 immunoreactivity (Fig. 2B). However, in *Ch25h*-deficient mice, there was a significant decrease in CD68 immunoreactivity (Fig. 2D), which is a marker of microglial phagolysosomes, suggesting that 25HC produced by *WT* microglia may limit phagolysosomal turnover. Since our data shows evidence for increased BBB permeability and infiltration of leukocytes into the brain parenchyma after LPS treatment (Fig. 6), it is possible that some of the CD68 staining may also result from infiltrating monocytes/macrophages. *Ch25h*-deficient mice also showed significantly decreased expression of the markers of microglial activation *Clec7a*, *Trem2*, and *Axl* (Fig. 3). Levels of 25HC in *WT* mice correlated strongly with IL-1β and moderately with IL-6 levels and only among *Ch25h*-expressing wild-type mice (Fig. 5C & I). The residual 25HC present among *KO* mice (Fig. 1C) is likely a product of non-enzymatic oxidation of cholesterol [52] and the activity of promiscuous enzymes such as CYP3A4 [28]. Our previous studies with primary mouse microglia showed that not only do *Ch25h*-deficient microglia produce lower levels of IL-1β, but addition of 25HC results in increased IL-1β production in response to LPS, suggesting that 25HC influences both expression and secretion of IL-1β [12]. Intriguingly, recent work has reported that *Ch25h*-deficient macrophages exhibit higher cholesterol synthesis upon LPS exposure that leads to increased mitochondrial membrane permeability and leakage of mitochondrial DNA that in turn results in elevated IL-1β secretion via the AIM2 inflammasome [53]. The underlying reasons for the opposing effects of *Ch25h* deficiency in microglia versus macrophages are unclear, but we speculate that other factors may influence myeloid cell physiology in a context- and cell-dependent manner.

Interestingly, brain levels of TNF did not substantially increase with LPS treatment (Fig. 5E), although prior research using a similar 1-hit LPS model had reported low but elevated TNF synthesis in mouse brain parenchyma using a more sensitive and precise cytometric bead assay [54]. Additionally, while cytokine secretion may have decreased over the prolonged LPS exposure over two days, expression of *Il1b*, *Il6*, *and Tnf* mRNAs remained upregulated by LPS treatment (Fig. 5A, D, & G).

In addition to 25HC-mediated changes in the inflammatory response of microglia, we also observed lower levels of astrocyte activation in LPS-treated *Ch25h*-deficient mice relative to wild-type mice. This underscores a potential role for 25HC in mediating microglia-astrocyte crosstalk. Many microglial factors, including cytokines (IL-1α, TNF), as well as other secreted factors, have been shown to mediate astrocyte activation [55, 56]. We recently showed that 25HC can dramatically modulate lipid metabolism in astrocytes via its inhibitory effect on SREBP-mediated gene expression and stimulation of LXRs [14]. Thus, it is possible that changes in astrocyte lipid metabolism due to 25HC secreted by microglia might play a role in astrocyte activation and/or function.

Disruption of the BBB is considered one of the key mechanisms underlying the neuroinflammation induced by systemic administration of LPS [33, 34]. Several effects of LPS on the BBB have been identified, such as direct interaction and structural damage of endothelial cells and additional components of the neurovascular unit [57]. LPS can also promote the release of cytokines and chemokines by peripheral immune cells that may induce structural remodeling of the BBB to enhance leukocyte migration and transport solutes to exacerbate neuroinflammation [58]. The induction of BBB permeability by systemic administration of LPS was demonstrated by enhanced transport of the small-sized BBB tracer sodium fluorescein similarly in *WT* and *KO* mice (Fig. 6G & H). Recent work has found that endothelial-specific knockout of *Ch25h* alleviates neuroinflammation in a model of multiple sclerosis [59]. Additionally, the *Ch25h* gene was identified as part of a gene expression module involved in BBB dysfunction; however, the effect size is small and the direction of the effect is ambiguous [60]. In contrast, our findings suggest *Ch25h*/25HC does not seem to play a role in the mechanisms underlying BBB permeability in our 2-hit LPS mouse model.

As mentioned, loss of BBB integrity can induce infiltration of leukocytes into the brain. Comparing 2, 5, or 7 consecutive days of administration of systemic LPS every 24 h, Thomson et al. found dramatic increases in the presence of neutrophils, NK cells, and NKT cells after two days of exposure to LPS, while recruitment of $CD8^+$ lymphocytes peaked after 5 days [24]. We also provided evidence of infiltration of the same leukocyte populations promoted by two consecutive days of LPS administration.

Further, our findings indicate that *Ch25h* expression may influence the infiltration of peripheral immune cells into the brain parenchyma mediated by LPS, specifically neutrophils and NK cells (Fig. 6C & E). Neutrophils are rapid responders to acute inflammation in the CNS and establish intercellular crosstalk with microglia that may exacerbate neuroinflammation in response to LPS administration [61]. Their small size, high nuclear deformability, and high migration speed relative to lymphocytes [24, 62] allow them to quickly infiltrate into the brain by transmigration through the BBB endothelial cells and return to the bloodstream to spread inflammatory signals to other peripheral immune cells [61]. Moreover, the most important inflammatory molecular mediator of neutrophil infiltration is IL-1 [62], a cytokine induced by LPS, the expression and production of which was found to be reduced by the absence of *Ch25h* and 25HC synthesis. Meanwhile, NK cells are important players in neuroinflammation mediated by systemic LPS. Early infiltration of NK cells promotes microglia expression of chemokines crucial for the recruitment of neutrophils into the brain, which in turn activate NK cells by secreting the neutrophil-specific protein, lactoferrin [63, 64]. Activated NK cells exert cytotoxicity in the brain by secretion of perforin and granzymes. In addition, they produce interferon-γ, a cytokine that amplifies glia responses and may promote a late recruitment of a variety of T lymphocytes [65]. Migration of NK cells into the CNS is directed by glial secreted chemokines such as CCL2, CXCL10, and CXCL12 [65]. Our data suggest that *Ch25h*/25HC may be involved in brain infiltration of NK cells (and possibly neutrophils) after LPS treatment. Based on our previous observation of decreased expression of *Cxcl10* in *Ch25h*-deficient microglia stimulated with tau fibrils [29], we speculate that 25HC may synergize with CXCL10 and/or other factors to promote NK cell chemotaxis into the brain. An additional hypothesis of how 25HC may promote leukocyte chemotaxis into the brain involves the metabolism of 25HC by CYP7B1 (a cytochrome P-450 enzyme) into 7α,25-dihydroxycholesterol (7α,25diHC) [66] which is a potent ligand for the chemotactic G-protein coupled receptor, GPR183/EBI2, that is expressed on leukocytes. 7α,25diHC has been shown to activate GPR183/EBI2 to mediate chemotaxis of B-cells [4] and infiltration of CD4+T-cells into the brain parenchyma in a mouse model of experimental autoimmune encephalomyelitis (EAE) [67]. Indeed, both 25HC-dependent mechanisms may synergize to mediate leukocyte chemotaxis into CNS parenchyma.

Intriguingly, while male and female mice similarly expressed markers of gliosis, females showed higher levels of cytokine production (Fig. 5). Importantly, as the only known product of the CH25H enzyme, levels of 25HC in the brain appeared to group by sex, with females forming a cluster of higher 25HC levels than males following LPS treatment (Fig. 5). However, the low number of samples per experimental group precludes firm conclusions about the statistical significance of these differences. No indication of sex differences was apparent in the low levels of 25HC independent of CH25H enzyme activity (i.e., 25HC levels that were observed in *ch25h*-/- mice) (Fig. 1C). The observed sex-specific clustering of 25HC levels also corresponded to differences in other neuroinflammatory transcriptomic markers (Figs. 4, S3, & S4) commensurate with previous work observing relatively higher neuroinflammation in females [68]. Likewise, women have a well-established higher risk of neurodegenerative diseases such as AD that persists even after accounting for the greater life expectancy of women [69]. The relationship between sex and inflammation is complex and age-dependent. 25HC is one of the many potential factors that may contribute to the sex differences observed in this study. While the underlying reasons for the relationship between 25HC and sex differences in inflammation are unclear, we speculate that 25HC may differentially influence the transcriptional regulation by nuclear receptors such as liver-x-receptor (LXR) and estrogen receptors (ERs). In fact, ER-mediated transrepression of proinflammatory pathways was found to be blocked by modulation of ERs by certain sterols [70]. Interestingly, 25HC has been reported to modulate ER-mediated transcription [71].

Together these findings support our observations that higher levels of 25HC in females may promote a greater inflammatory response. Whether 25HC contributes significantly to sex differences in AD and other diseases where neuroinflammation is prominent will require future investigation.

Conclusions

Our findings demonstrate that 25HC is a proinflammatory promoter of brain cytokine production and leukocyte infiltration in a mouse model of LPS-mediated neuroinflammation.

Limitations of this study

In this study, we used a global knockout of *Ch25h*; therefore, it is unclear whether all observed effects are mediated by *Ch25h* in the brain as some of the effects may be mediated by changes in the peripheral immune response. Moreover, considering the vast existing literature examining the effects of LPS on peripheral systems, our study did not analyze changes in immune response and gut microbiome triggered by intraperitoneal administration of LPS. While our data suggests that *Ch25h*/25HC contribute to sex differences in inflammatory response against LPS challenge, additional factors are likely to contribute to sex differences. The relatively smaller sample

size of each group in this study limits confident ascertainment of sex differences. Further, while we show that *Ch25h* deficiency reduces NK cell migration to the CNS, the exact roles of 25HC or its downstream metabolite 7α,25-diHC must be clarified with additional studies.

Materials and methods

Mouse model of LPS-induced neuroinflammation

Wild-type (C57BL/6J, #000664) and *ch25h-/-* (*KO*, #016263) mice were purchased from The Jackson Laboratory and maintained as homozygotes. Absence of the *Ch25h* gene in *KO* mice and its presence in *WT* mice was corroborated using TransnetYX automated genotyping services (Memphis, Tennessee, USA).

At 23–26 weeks of age, mice from the same genotype were randomly assigned to one of the two treatments (PBS or LPS), keeping an equal distribution of mice per sex. Mice were intraperitoneally (i.p.) administered with LPS (2 mg/kg per dose) or vehicle (PBS) twice with a 24-hour interval in a blinded manner (Fig. 1A). All the injected animals survived the 2-hit model treatment and were perfused 24 h after the last injection. A total of 40 mice (including $n=5$ per genotype per sex per treatment) were used with no unexpected deaths until perfusion and tissue collection. The left hemisphere was fixed in 4% paraformaldehyde. Hippocampus (for RNA extraction) and cortex (for protein and oxysterol measurements) were dissected from the right hemisphere and were frozen at -80˚C until use. Experiments were conducted fully blind to genotype and treatment until after the results were analyzed.

All animal procedures and experiments were performed under guidelines approved by the animal studies committee at Washington University School of Medicine.

Immunofluorescence staining

Left-hemisphere tissue sections from wild-type and *Ch25h* knockout mice were sliced at a thickness of 40 microns using a cryostat (Thermo Fisher microm 430). Slices were then placed in a cryoprotectant (30% ethylene-glycol, 15% sucrose in PBS) and stored at -20˚C until use for immunostaining. Two slices 960 mm apart were taken from each animal (4 animals/treatment group). The sections were washed in Tris-buffered saline (TBS) 3 times for 5 min each. Sections were then placed in a blocking solution made of 3% goat serum, 3% bovine serum albumin (BSA), and 0.25% Triton X-100 in TBS for 1 h. Sections were then incubated with the primary antibody cocktail against CD68 (rat monoclonal; 1:250; catalog no. MCA1957; Bio-rad), GFAP (Chicken polyclonal; 1:1000; catalog no. Ab4674; Abcam), and IBA1 (Polyclonal rabbit; 1:500; catalog no. 019-19741; Waco) in TBS containing 1% goat serum and 1% BSA. The sections were left overnight at 4˚C. The next day, tissue sections were washed three times with fresh TBS for 5 min each. The tissue sections were then placed in the secondary antibody cocktail containing 1:1,000 dilution each of DAPI, goat anti-rat-Alexa555 (Invitrogen; Catalog no. A21434), goat anti-chicken-Alexa 647 (Invitrogen; Catalog no. A21449), and goat anti-rabbit-Alexa488 (Invitrogen; Catalog no. A32731) in TBS. (Primary and secondary antibody cocktails were centrifuged at 10,000 rpm for 5 min to remove insoluble particulate matter prior to use. The stained sections were then washed three times with TBS for 7 min each. The slices were mounted in low light in mounted using FluoroShield mounting media (Sigma-Aldrich; Product no. F6182).

Imaging

Images were retrieved using a Nikon spinning disk confocal microscope. Using Fiji, a region of interest (ROI) around the hippocampus was drawn. Background subtraction was conducted using a 50-pixel rolling ball. Using batch processing, the same threshold settings were applied to all the images of each individual stain, and area fraction was measured. The area fraction from the 2 sections analyzed per mouse brain were averaged and plotted as an individual value. After the analyses, the representative image for each genotype and treatment was selected according to the mean value per group. For visual purpose, only the dentate gyrus region (ROI 200 microns x 200 microns) is shown.

Preparation of tissue extracts

Frozen cortical tissue was homogenized with a micropestle and electric rotor in 200 µL of mammalian protein extraction reagent (M-PER) (Thermo Scientific, Cat. #: 78501) containing ProBlock Gold Extra Strength Protease Inhibitor Cocktail Kit (GoldBio, Cat. #: GB-116-2). The cortical lysate was then aliquoted into a 96-well plate and stored at -80 °C for future cytokine estimation.

Enzyme-linked immunosorbent assay (ELISA)

ELISA kits from R&D Systems were used to quantify various cytokines, including IL-1β (Cat #: DY401-05), TNF (Cat #: DY410-05), and IL-6 (Cat #: DY40605) in the posterior cortical lysates of the *WT* and *KO* mice. The assays were performed as instructed in the manufacturer's protocols, except ELISA steps were performed in half-well rather than full-well plates (Corning Cat#: 3690) with half of the volume in each well (50 µL instead of 100 µL).

RNA extraction

Frozen hippocampal tissue was homogenized with a micropestle and electric rotor in RNA Lysis Buffer from Zymo Research (Cat#: R2060-1-100) before immediately proceeding with RNA extraction using the Zymo Research Quick-RNA MiniPrep Plus kit (Cat. #:

R1058) according to the manufacturer's instructions. After eluting the RNA into nuclease-free water, the RNA concentrations were measured using a NanoDrop spectrophotometer.

Reverse transcription cDNA synthesis & quantitative polymerase chain reaction (qPCR)

The High-Capacity cDNA Reverse Transcription with RNase Inhibitor Kit (Applied Biosystems, Cat. #: 4474966) was used to reverse transcribe 100-200ng of RNA from mouse hippocampus in accordance with the manufacturer's instructions. For the qPCR reaction mix, PrimeTime probe-based qPCR assays (see Suppl. Table V) and PrimeTime Gene Expression Master mix (IDT, Cat# 1055771) were obtained from IDT (Integrated DNA Technologies, Inc). qPCR reactions were run using the "Fast" mode on a QuantStudio™ 3 Real-Time PCR Instrument (Applied Biosystems by ThermoFisher, A28131). Probes and primers used for various genes are listed in Supplementary Table V. Data were normalized against actin (Actb) and the $2^{-\Delta\Delta Ct}$ method was used to calculate relative gene expression value (Relative Quantification, RQ).

RNA sequencing and analysis

Samples were prepared according to library kit manufacturer's protocol, indexed, pooled, and sequenced on an Illumina NovaSeq 6000. Basecalls and demultiplexing were performed with Illumina's bcl2fastq2 software. RNA-seq reads were then aligned and quantitated to the Ensembl release 101 primary assembly with an Illumina DRAGEN Bio-IT on-premise server running version 3.9.3-8 software.

All gene counts were then imported into the R/Bioconductor package EdgeR [72] and TMM normalization size factors were calculated to adjust for samples for differences in library size. Ribosomal genes and genes not expressed greater than one count-per-million in the smallest group size minus one sample were excluded from further analysis. The TMM size factors and the matrix of counts were then imported into the R/Bioconductor package Limma [73]. Weighted likelihoods based on the observed mean-variance relationship of every gene and sample were then calculated for all samples and the count matrix was transformed to moderated log 2 counts-per-million with Limma's voomWithQualityWeights [74]. The performance of all genes was assessed with plots of the residual standard deviation of every gene to their average log-count with a robustly fitted trend line of the residuals. Differential expression analysis was then performed to analyze for differences between conditions and the results were filtered for only those genes with Benjamini-Hochberg false-discovery rate adjusted p-values less than or equal to 0.05. For LPS effects, the following comparisons were performed: female *KO* mice treated with LPS were compared to those treated with PBS, male *KO* mice treated with LPS were compared to those treated with PBS, female *WT* mice treated with LPS were compared to those treated with PBS, and male *WT* mice treated with LPS were compared to those treated with PBS. For gender differences, female *KO* mice treated with LPS were compared to male *KO* mice treated with LPS, female *KO* mice treated with PBS were compared to male *KO* mice treated with PBS, female *WT* mice treated with LPS were compared to male *WT* mice treated with LPS, female *WT* mice treated with PBS were compared to male *WT* mice treated with PBS. For each contrast extracted with Limma, biological enrichment was carried out with the web tool "Metascape" to identify significantly enriched Gene Ontology (GO) terms [75]. Pathway maps were generated using Cytoscape [76].

Liquid chromatography-mass spectrometry (LC/MS)

Brain samples from 40 mice were profiled for oxysterols (3β, 5α, 6β-trihydroxycholestane (Triol), and 7-ketocholesterol (7-KC), 4β-hydroxycholesterol (4β-HOC), 7αhydroxycholesterol (7α-HOC), 7β-hydroxycholesterol (7β-HOC), 24-hydroxycholesterol (24-HOC), 25-hydroxycholesterol (25-HOC), and 27-hydroxycholesterol (27-HOC)). The brain samples were homogenized in water (20 mL/g tissue) using Omni Bead Ruptor 24 (Omni International, Inc.). The oxysterols in 50 µL of homogenate were extracted with liquid-liquid extraction after addition of Triol-d7, 7-KC-d7, 4β-HOC-d7, 7α-HOC-d7, 7βHOC–d7, 24-HOC–d7, 25-HOC-d6, 27-HOC–d5 as the internal standards. The oxysterols and their internal standards were derivatized with nicotinic acid to increase their mass spectrometric sensitivities. Quality control (QC) samples were prepared by pooling a portion of study samples and injecting every 5 samples to monitor instrument performance. The sample analysis was performed with a Shimadzu 20AD HPLC system coupled to a 4000QTRAP mass spectrometer operated in positive multiple reaction monitoring mode. Data processing was conducted with Analyst 1.6.3.

In vivo assessment of blood-brain barrier permeability

The 2-hit LPS paradigm was performed on a new cohort of mice (a total of 40 mice, including $n=5$ per genotype per sex per treatment identical to the methods described in 'Mouse model of LPS-induced neuroinflammation') to assess BBB permeability and quantify the infiltration of leukocytes into the brain. According to a previously published method [35], one day after the second LPS-hit, mice were injected (subcutaneous) with 100 µl of 100 mg/ml sodium fluorescein (NaFl) salt (Sigma-Aldrich, F6377) in PBS. After 45 min, mice were euthanized by cardiac perfusion with DPBS, followed by collection of blood for

serum isolation. The brain was harvested, the left hemisphere was dissected in hippocampus and cortex to estimate the amount of NaFl penetration throughout the CNS. Serum was used to normalize for circulating levels of the NaFl in the peripheral blood, which was diluted in PBS (1:200). Tissues were homogenized in 500 µl of PBS and all samples were diluted 1:1 in 2% trichloroacetic acid (Sigma-Aldrich, T0699) and incubated overnight at 4 °C to precipitate protein, followed by a centrifugation at 4,000 g at 4ºC for 15 min. Supernatants were diluted in equal volumes of borate buffer solution (Honeywell Fluka, 33650). Fluorescence emission at 538 nm was measured on Cytation 5 Imaging Reader (BioTek Instruments, Inc.) using the Gen 5 software. Fluorescein emission values were normalized to tissue weight and serum values for each individual mouse.

Single cell isolation and flow cytometry analysis

Hippocampus and cortex from the right hemisphere of mice injected with sodium fluorescein were dissected and freshly used to obtain a single cell suspension for analysis of leukocytes in the brain by flow cytometry. Briefly, tissue was minced in cold-DPBS. A subsequent enzymatic digestion with Collagenase IV (2 mg/ml, Gibco™, 17104019) and DNase I (2 mg/ml, Sigma-Aldrich, DN25-1G) was conducted at 37 °C for 30 min. Homogenates were passed through a 70 mm cell strainer (Corning, CLS431751) and centrifuged for 7 min at 350 g at 4ºC. The pellet was resuspended in 40% Percoll and centrifuged for 10 min at 1000 g at 4ºC to remove debris and myelin. Further, single cells were resuspended in prechilled FACS buffer (2mM EDTA/0.5% BSA/PBS) and incubated with anti-CD16/32 (Fc block 1:200, Leinco Technologies, C247) for 10 min. Cells were incubated with the next fluorescent conjugated antibodies at 4ºC for 15 min: Brilliant Violet 510 anti-mouse CD45 (1:200, Biolegend, B372553), APC/Cyanine7 anti-mouse/human CD11b (1:200, Biolegend, B381128), APC anti-Mouse TCR β (1:200, BD, BDB553174), PE anti-mouse NK-1.1 (1:200, Biolegend, B367623), and Pacific Blue anti-mouse Ly-6G (1:200, Biolegend, B380041). Cells were analyzed using a BD FACSCanto II™ flow cytometry system (BD Biosciences, San Jose, CA). Data were analyzed using FlowJo™ 10 (BD Biosciences, San Jose, CA). Cell population proportions were normalized by total number of single cells.

Statistical analysis

Data are presented as mean ± SD. GraphPad Prism 9.2 was used to perform statistical analyses. Gaussian distribution was evaluated using the D'Agostino & Pearson normality test. Differences between groups were evaluated by two-way ANOVA with Fisher's least significant difference (LSD) post-hoc test.

Abbreviations

LPS	Lipopolysaccharide
AD	Alzheimer's disease
TLR4	Toll-like receptor-4
CH25H	Cholesterol-25-hydroxylase
25HC	25-hydroxycholesterol
7a,25diHC	7a,25-dihydroxycholesterol
DAM	Disease-associated microglia

Supplementary Information

The online version contains supplementary material available at https://doi.org/10.1186/s12974-024-03233-1.

Supplementary Material 1: **Figure S1** Quantification of the two structural isomers of 25HC. Quantitation of 24-(S)-HC (A) and 27-HC (B) in PBS- and LPS-injected wildtype (*WT*) and *Ch25h*-deficient (*KO*) mouse brains. Male mice are indicated in blue, and female mice are in orange. Data are presented as mean values ± SD ($n = 5$ per sex per genotype per treatment group). Statistical significance was defined using a two-way ANOVA with Fisher's LSD post-hoc multiple comparisons test (**$P < 0.01$ & ***$P < 0.001$).

Supplementary Material 2: **Figure S2** Expression of *Cyp7b1*. (A) Schematic of 25HC pathway leading to chemoattraction of GPR183 expressing leukocytes. (B) Relative expression of *Cyp7b1* mRNA measured by qPCR. Data are presented as mean values ± SD ($n = 5$ per sex per genotype per treatment group). Statistical significance was defined using a two-way ANOVA with Fisher's LSD post-hoc multiple comparisons test (*$P < 0.05$, **$P < 0.01$, & ***$P < 0.001$).

Supplementary Material 3: **Figure S3** Transcriptomic data. (A) Principal component analysis (PCA) of RNA-seq measurements from 40 experimental mice ($n = 5$ per sex per genotype per treatment group), sorted by sex, treatment condition, and *Ch25h* genotype. One sample was an outlier and was excluded from further analysis. (B-E) Volcano plots of differentially expressed genes (DEGs) in these animals. DEGs were defined as those with fold-change >= 2 at adjusted p-value (q-value) < 0.05.

Supplementary Material 4: **Figure S4** Bar graph of enriched gene ontology (GO) terms for the differentially upregulated gene lists across all groups, colored by P-values. P-values are also shown on the X-axis.

Supplementary Material 5: **Figure S5** Role of CH25H/25HC in neutrophil and T lymphocyte recruitment mediated by LPS. Infiltration of neutrophils into the brain of PBS- and LPS-injected *WT* and *KO* mice were determined by analyzing the neutrophil-specific marker LY6G. (A) Relative expression of *Ly6g* mRNA measured by qPCR in the hippocampus and (B) the correlation between Ly6g relative expression and 25HC levels. 25HC concentrations are as shown in Fig. 1C. Data are presented as mean values ± SD ($n = 5$ per sex per genotype per treatment group). (C) Representative immunofluorescence images of mouse hippocampal sections stained for LY6G (red); nuclei were stained with DAPI (blue). (D) Percentage of area covered by LY6G in the hippocampus. Infiltration of T lymphocytes were analyzed by immunofluorescence using an anti-CD3 antibody (representative images not shown). (E) Percentage of area covered by CD3 in the hippocampus is shown. Data are presented as mean values ± SD ($n = 4$ per sex per genotype per treatment group). Male mice are indicated in blue and female mice are in orange. Statistical significance was defined using a two-way ANOVA with Fisher's LSD post-hoc multiple comparisons test (**$P < 0.01$, ***$P < 0.001$, & ****$P < 0.0001$). Statistical significance and slope of the line were calculated with simple linear regression analysis and correlations were assessed by calculating the coefficient of determination (R^2).

Supplementary Material 6: **Supplementary table I** Size of gene-lists influenced by gender and genotype.

Supplementary Material 7: **Supplementary table II** Differential gene expression between females and males.

Supplementary Material 8: **Supplementary table III** Gene ontology analysis of differentially expressed genes.

Supplementary Material 9: **Supplementary table IV** Comparisons of the downregulated genes and pathways in response to LPS treatment.

Supplementary Material 10: **Supplementary table V** Sequences of primers used for qPCR analysis.

Acknowledgements
We acknowledge technical assistance from Kaylee Stillwell, technical advice and assistance from Jennifer Lawrence, PhD, and from Washington University core facilities.

Author contributions
AGC: conceived and designed the research studies; JR, DTR, AGC: performed experiments and acquired data; JR, DTR, JY, AGC: analyzed the data; JR, AGC, DTR: wrote the paper; JR, DTR, SMP, AGC: edited the manuscript.

Funding
This study was partially funded by Sage Therapeutics, Cambridge, MA. Sage Therapeutics had no role in the conceptualization, design, data collection, analysis, decision to publish, or preparation of the manuscript. Research reported in this publication was partially supported by the National Institute on Aging of the National Institutes of Health under Award Number R01AG081419. The content is solely the responsibility of the authors and does not necessarily represent the official views of the National Institutes of Health.

Data availability
No datasets were generated or analysed during the current study.

Declarations

Ethics approval and consent to participate
Research using mouse as a model system of neuroinflammation was approved by the Institutional Animal Care and Use Committee (IACUC) of the Washington University School of Medicine.

Consent for publication
Not applicable.

Competing interests
The authors declare no competing interests.

Received: 22 July 2024 / Accepted: 12 September 2024
Published online: 05 October 2024

References

1. Chen Y, Dai J, Tang L, et al. Neuroimmune transcriptome changes in patient brains of psychiatric and neurological disorders. Mol Psychiatry. 2023;28(2):710–21. https://doi.org/10.1038/s41380-022-01854-7.
2. Colonna M, Brioschi S. Neuroinflammation and neurodegeneration in human brain at single-cell resolution. Nat Rev Immunol. 2020;20(2):81–2. https://doi.org/10.1038/s41577-019-0262-0.
3. Xing C, Huang X, Wang D, Yu D, Hou S, Cui H, et al. Roles of bile acids signaling in neuromodulation under physiological and pathological conditions. Cell Biosci. 2023;13(1):106.
4. Hannedouche S, Zhang J, Yi T, et al. Oxysterols direct immune cell migration via EBI2. Nature. 2011;475(7357):524–7. https://doi.org/10.1038/nature10280.
5. Reboldi A, Dang EV, McDonald JG, Liang G, Russell DW, Cyster JG. 25-Hydroxycholesterol suppresses interleukin-1–driven inflammation downstream of type I interferon. Science. 2014;345(6197):679–84. https://doi.org/10.1126/science.1254790.
6. Liu SY, Aliyari R, Chikere K, et al. Interferon-Inducible cholesterol-25-Hydroxylase broadly inhibits viral entry by production of 25-Hydroxycholesterol. Immunity. 2013;38(1):92–105. https://doi.org/10.1016/j.immuni.2012.11.005.
7. Zhang Y, Chen K, Sloan SA, et al. An RNA-Sequencing transcriptome and Splicing Database of Glia, neurons, and vascular cells of the cerebral cortex. J Neurosci. 2014;34(36):11929–47. https://doi.org/10.1523/JNEUROSCI.1860-14.2014.
8. Zhang Y, Sloan SA, Clarke LE, et al. Purification and characterization of progenitor and mature human astrocytes reveals transcriptional and functional differences with Mouse. Neuron. 2016;89(1):37–53. https://doi.org/10.1016/j.neuron.2015.11.013.
9. Bauman DR, Bitmansour AD, McDonald JG, Thompson BM, Liang G, Russell DW. 25-Hydroxycholesterol secreted by macrophages in response to Toll-like receptor activation suppresses immunoglobulin A production. *Proceedings of the National Academy of Sciences*. 2009;106(39):16764–16769. https://doi.org/10.1073/pnas.0909142106
10. Keren-Shaul H, Spinrad A, Weiner A, et al. A Unique Microglia Type Associated with Restricting Development of Alzheimer's Disease. Cell. 2017;169(7):1276–e129017. https://doi.org/10.1016/j.cell.2017.05.018.
11. Krasemann S, Madore C, Cialic R, et al. The TREM2-APOE pathway drives the Transcriptional phenotype of dysfunctional microglia in neurodegenerative diseases. Immunity. 2017;47(3):566–e5819. https://doi.org/10.1016/j.immuni.2017.08.008.
12. Wong MY, Lewis M, Doherty JJ, et al. 25-Hydroxycholesterol amplifies microglial IL-1β production in an apoE isoform-dependent manner. J Neuroinflammation. 2020;17(1):192. https://doi.org/10.1186/s12974-020-01869-3.
13. Cyster JG, Dang EV, Reboldi A, Yi T. 25-Hydroxycholesterols in innate and adaptive immunity. Nat Rev Immunol. 2014;14(11):731–43. https://doi.org/10.1038/nri3755.
14. Cashikar A, Rios D, Timm D, et al. Regulation of astrocyte lipid metabolism and ApoE secretion by the microglial oxysterol, 25-hydroxycholesterol. J Lipid Res Published Online Febr. 2023;25:100350. https://doi.org/10.1016/j.jlr.2023.100350.
15. Koarai A, Yanagisawa S, Sugiura H, et al. 25-hydroxycholesterol enhances cytokine release and toll-like receptor 3 response in airway epithelial cells. Respir Res. 2012;13(1):63. https://doi.org/10.1186/1465-9921-13-63.
16. Gold ES, Diercks AH, Podolsky I, et al. 25-Hydroxycholesterol acts as an amplifier of inflammatory signaling. Proc Natl Acad Sci. 2014;111(29):10666–71. https://doi.org/10.1073/pnas.1404271111.
17. Guo C, Chi Z, Jiang D, et al. Cholesterol homeostatic Regulator SCAP-SREBP2 integrates NLRP3 inflammasome activation and cholesterol Biosynthetic Signaling in macrophages. Immunity. 2018;49(5):842–e8567. https://doi.org/10.1016/j.immuni.2018.08.021.
18. Diczfalusy U, Olofsson KE, Carlsson AM, et al. Marked upregulation of cholesterol 25-hydroxylase expression by lipopolysaccharide. J Lipid Res. 2009;50(11):2258–64. https://doi.org/10.1194/jlr.M900107-JLR200.
19. Oliveira-Lima OC, Carvalho-Tavares J, Rodrigues MF, et al. Lipid dynamics in LPS-induced neuroinflammation by DESI-MS imaging. Brain Behav Immun. 2019;79:186–94. https://doi.org/10.1016/j.bbi.2019.01.029.
20. Blank M, Enzlein T, Hopf C. LPS-induced lipid alterations in microglia revealed by MALDI mass spectrometry-based cell fingerprinting in neuroinflammation studies. Sci Rep. 2022;12(1):2908. https://doi.org/10.1038/s41598-022-06894-1.
21. Dawson TM, Golde TE, Lagier-Tourenne C. Animal models of neurodegenerative diseases. Nat Neurosci. 2018;21(10):1370–9. https://doi.org/10.1038/s41593-018-0236-8.
22. Ransohoff RM. Animal models of multiple sclerosis: the good, the bad and the bottom line. Nat Neurosci. 2012;15(8):1074–7. https://doi.org/10.1038/nn.3168.
23. Qin L, Wu X, Block ML, et al. Systemic LPS causes chronic Neuroinflammation and Progressive Neurodegeneration. Glia. 2007;55(5):453–62. https://doi.org/10.1002/glia.20467.
24. Thomson CA, McColl A, Graham GJ, Cavanagh J. Sustained exposure to systemic endotoxin triggers chemokine induction in the brain followed by a rapid influx of leukocytes. J Neuroinflamm. 2020;17(1):94. https://doi.org/10.1186/s12974-020-01759-8.
25. Park K, Scott AL. Cholesterol 25-hydroxylase production by dendritic cells and macrophages is regulated by type I interferons. J Leukoc Biol. 2010;88(6):1081–7. https://doi.org/10.1189/jlb.0610318.
26. Izumi Y, Cashikar AG, Krishnan K, et al. A proinflammatory stimulus disrupts hippocampal plasticity and learning via Microglial activation and 25-Hydroxycholesterol. J Neurosci. 2021;41(49):10054–64. https://doi.org/10.1523/JNEUROSCI.1502-21.2021.
27. Srinivasan K, Friedman BA, Etxeberria A, et al. Alzheimer's patient microglia exhibit enhanced aging and unique transcriptional activation. Cell Rep. 2020;31(13):107843. https://doi.org/10.1016/j.celrep.2020.107843.
28. Honda A, Miyazaki T, Ikegami T, et al. Cholesterol 25-hydroxylation activity of CYP3A. J Lipid Res. 2011;52(8):1509–16. https://doi.org/10.1194/jlr.M014084.
29. Toral-Rios D, Long JM, Ulrich JD, et al. Cholesterol 25-hydroxylase mediates neuroinflammation and neurodegeneration in a mouse model of tauopathy. J Exp Med. 2024;221(4):e20232000. https://doi.org/10.1084/jem.20232000.

30. Monson EA, Crosse KM, Duan M, et al. Intracellular lipid droplet accumulation occurs early following viral infection and is required for an efficient interferon response. Nat Commun. 2021;12(1):4303. https://doi.org/10.1038/s41467-021-24632-5.
31. Marschallinger J, Iram T, Zardeneta M, et al. Lipid-droplet-accumulating microglia represent a dysfunctional and proinflammatory state in the aging brain. Nat Neurosci. 2020;23(2):194–208. https://doi.org/10.1038/s41593-019-0566-1.
32. Chen X, Firulyova M, Manis M, et al. Microglia-mediated T cell infiltration drives neurodegeneration in tauopathy. Nature. 2023;615(7953):668–77. https://doi.org/10.1038/s41586-023-05788-0.
33. Eckman PL, King WM, Brunson JG. Studies on the blood brain barrier. I. effects produced by a single injection of gramnegative endotoxin on the permeability of the cerebral vessels. Am J Pathol. 1958;34(4):631–43.
34. Allen IV, THE EFFECT OF BACTERIAL PYROGEN ON THE BLOOD-BRAIN. BARRIER FOR TRYPAN BLUE. J Pathol Bacteriol. 1965;89:481–94.
35. Lawrence JH, Patel A, King MW, Nadarajah CJ, Daneman R, Musiek ES. Microglia drive diurnal variation in susceptibility to inflammatory blood-brain barrier breakdown. bioRxiv. 2024. https://doi.org/10.1101/2024.04.10.588924.
36. Wispelwey B, Lesse AJ, Hansen EJ, Scheld WM. Haemophilus influenzae lipopolysaccharide-induced blood brain barrier permeability during experimental meningitis in the rat. J Clin Invest. 1988;82(4):1339–46. https://doi.org/10.1172/JCI113736.
37. Kwon HS, Koh SH. Neuroinflammation in neurodegenerative disorders: the roles of microglia and astrocytes. Translational Neurodegeneration. 2020;9(1):42. https://doi.org/10.1186/s40035-020-00221-2.
38. Leng F, Edison P. Neuroinflammation and microglial activation in Alzheimer disease: where do we go from here? Nat Rev Neurol. 2021;17(3):157–72. https://doi.org/10.1038/s41582-020-00435-y.
39. Heneka MT, Golenbock DT, Latz E. Innate immunity in Alzheimer's disease. Nat Immunol. 2015;16(3):229–36. https://doi.org/10.1038/ni.3102.
40. Marsh SE, Abud EM, Lakatos A et al. The adaptive immune system restrains Alzheimer's disease pathogenesis by modulating microglial function. *Proceedings of the National Academy of Sciences*. 2016;113(9):E1316-E1325. https://doi.org/10.1073/pnas.1525466113
41. Chen X, Holtzman DM. Emerging roles of innate and adaptive immunity in Alzheimer's disease. Immunity. 2022;55(12):2236–54. https://doi.org/10.1016/j.immuni.2022.10.016.
42. Holmes C, Cunningham C, Zotova E, et al. Systemic inflammation and disease progression in Alzheimer disease. Neurology. 2009;73(10):768–74. https://doi.org/10.1212/WNL.0b013e3181b6bb95.
43. Semmler A, Widmann CN, Okulla T, et al. Persistent cognitive impairment, hippocampal atrophy and EEG changes in sepsis survivors. J Neurol Neurosurg Psychiatry. 2013;84(1):62–9. https://doi.org/10.1136/jnnp-2012-302883.
44. Maheshwari P, Eslick GD. Bacterial infection and Alzheimer's Disease: a Meta-analysis. J Alzheimer's Disease. 2015;43(3):957–66. https://doi.org/10.3233/JAD-140621.
45. Itzhaki RF. Overwhelming evidence for a major role for Herpes Simplex Virus Type 1 (HSV1) in Alzheimer's Disease (AD); underwhelming evidence against. Vaccines (Basel). 2021;9(6):679. https://doi.org/10.3390/vaccines9060679.
46. Levine KS, Leonard HL, Blauwendraat C, et al. Virus exposure and neurodegenerative disease risk across national biobanks. Neuron. 2023;111(7):1086–e10932. https://doi.org/10.1016/j.neuron.2022.12.029.
47. Seo Doh, O'Donnell D, Jain N, et al. ApoE isoform– and microbiota-dependent progression of neurodegeneration in a mouse model of tauopathy. Science. 2023;379(6628):eadd1236. https://doi.org/10.1126/science.add1236.
48. Okun E, Griffioen KJ, Lathia JD, Tang SC, Mattson MP, Arumugam TV. Toll-like receptors in neurodegeneration. Brain Res Rev. 2009;59(2):278–92. https://doi.org/10.1016/j.brainresrev.2008.09.001.
49. Song M, Jin J, Lim JE, et al. TLR4 mutation reduces microglial activation, increases Aβ deposits and exacerbates cognitive deficits in a mouse model of Alzheimer's disease. J Neuroinflammation. 2011;8:92. https://doi.org/10.1186/1742-2094-8-92.
50. Campolo M, Paterniti I, Siracusa R, Filippone A, Esposito E, Cuzzocrea S. TLR4 absence reduces neuroinflammation and inflammasome activation in Parkinson's diseases in vivo model. Brain Behav Immun. 2019;76:236–47. https://doi.org/10.1016/j.bbi.2018.12.003.
52. Ide M, Harris M, Stevens A, et al. Periodontitis and Cognitive decline in Alzheimer's Disease. PLoS ONE. 2016;11(3):e0151081. https://doi.org/10.1371/journal.pone.0151081.
52. Shi Q, Zhan T, Bi X, Ye B, ce, Qi N. Cholesterol-autoxidation metabolites in host defense against infectious diseases. Eur J Immunol. 2023;53(9):2350501. https://doi.org/10.1002/eji.202350501.
53. Dang EV, McDonald JG, Russell DW, Cyster JG. Oxysterol restraint of cholesterol synthesis prevents AIM2 inflammasome activation. Cell. 2017;171(5):1057–e107111. https://doi.org/10.1016/j.cell.2017.09.029.
54. Cazareth J, Guyon A, Heurteaux C, Chabry J, Petit-Paitel A. Molecular and cellular neuroinflammatory status of mouse brain after systemic lipopolysaccharide challenge: importance of CCR2/CCL2 signaling. J Neuroinflamm. 2014;11(1):132. https://doi.org/10.1186/1742-2094-11-132.
55. Liddelow SA, Guttenplan KA, Clarke LE, et al. Neurotoxic reactive astrocytes are induced by activated microglia. Nature. 2017;541(7638):481–7. https://doi.org/10.1038/nature21029.
56. Liddelow SA, Barres BA. Reactive Astrocytes: Production, Function, and, Potential T. *Immunity*. 2017;46(6):957–967. https://doi.org/10.1016/j.immuni.2017.06.006
57. Erickson MA, Shulyatnikova T, Banks WA, Hayden MR. Ultrastructural remodeling of the blood–brain barrier and neurovascular unit by Lipopolysaccharide-Induced Neuroinflammation. Int J Mol Sci. 2023;24(2):1640. https://doi.org/10.3390/ijms24021640.
58. Galea I. The blood–brain barrier in systemic infection and inflammation. Cell Mol Immunol. 2021;18(11):2489–501. https://doi.org/10.1038/s41423-021-00757-x.
59. Ruiz F, Peter B, Rebeaud J, et al. Endothelial cell-derived oxysterol ablation attenuates experimental autoimmune encephalomyelitis. EMBO Rep. 2023;24(3):e55328. https://doi.org/10.15252/embr.202255328.
60. Munji RN, Soung AL, Weiner GA, et al. Profiling the mouse brain endothelial transcriptome in health and disease models reveals a core blood–brain barrier dysfunction module. Nat Neurosci. 2019;22(11):1892–902. https://doi.org/10.1038/s41593-019-0497-x.
61. Kim YR, Kim YM, Lee J, Park J, Lee JE, Hyun YM. Neutrophils return to Bloodstream through the brain blood Vessel after Crosstalk with Microglia during LPS-Induced Neuroinflammation. Front Cell Dev Biol. 2020;8:613733. https://doi.org/10.3389/fcell.2020.613733.
62. Ching S, He L, Lai W, Quan N. IL-1 type I receptor plays a key role in mediating the recruitment of leukocytes into the central nervous system. Brain Behav Immun. 2005;19(2):127–37. https://doi.org/10.1016/j.bbi.2004.06.001.
63. Shau H, Kim A, Golub SH. Modulation of natural killer and lymphokine-activated killer cell cytotoxicity by lactoferrin. J Leukoc Biol. 1992;51(4):343–9. https://doi.org/10.1002/jlb.51.4.343.
64. He H, Geng T, Chen P, et al. NK cells promote neutrophil recruitment in the brain during sepsis-induced neuroinflammation. Sci Rep. 2016;6(1):27711. https://doi.org/10.1038/srep27711.
65. Ning Z, Liu Y, Guo D, Lin WJ, Tang Y. Natural killer cells in the central nervous system. Cell Commun Signal. 2023;21(1):341. https://doi.org/10.1186/s12964-023-01324-9.
66. Schwarz M, Lund EG, Lathe R, Björkhem I, Russell DW. Identification and characterization of a mouse oxysterol 7α-Hydroxylase cDNA*. J Biol Chem. 1997;272(38):23995–4001. https://doi.org/10.1074/jbc.272.38.23995.
67. Wanke F, Moos S, Croxford AL, et al. EBI2 is highly expressed in multiple sclerosis lesions and promotes early CNS Migration of Encephalitogenic CD4 T cells. Cell Rep. 2017;18(5):1270–84. https://doi.org/10.1016/j.celrep.2017.01.020.
68. Yang Y, Kozloski M. Sex differences in Age trajectories of physiological dysregulation: inflammation, metabolic syndrome, and allostatic load. Journals Gerontology: Ser A. 2011;66A(5):493–500. https://doi.org/10.1093/gerona/glr003.
69. Chêne G, Beiser A, Au R, et al. Gender and incidence of dementia in the Framingham Heart Study from mid-adult life. Alzheimer's Dement. 2015;11(3):310–20. https://doi.org/10.1016/j.jalz.2013.10.005.
70. Saijo K, Collier JG, Li AC, Katzenellenbogen JA, Glass CK. An ADIOL-ERβ-CtBP transrepression pathway negatively regulates microglia-mediated inflammation. Cell. 2011;145(4):584–95. https://doi.org/10.1016/j.cell.2011.03.050.
71. Lappano R, Recchia AG, Francesco EMD, et al. The cholesterol metabolite 25-Hydroxycholesterol activates estrogen receptor α-Mediated signaling in Cancer cells and in Cardiomyocytes. PLoS ONE. 2011;6(1):e16631. https://doi.org/10.1371/journal.pone.0016631.
72. Robinson MD, McCarthy DJ, Smyth GK. edgeR: a Bioconductor package for differential expression analysis of digital gene expression data. Bioinformatics. 2010;26(1):139–40. https://doi.org/10.1093/bioinformatics/btp616.

73. Ritchie ME, Phipson B, Wu D, et al. Limma powers differential expression analyses for RNA-sequencing and microarray studies. Nucleic Acids Res. 2015;43(7):e47. https://doi.org/10.1093/nar/gkv007.
74. Liu R, Holik AZ, Su S, et al. Why weight? Modelling sample and observational level variability improves power in RNA-seq analyses. Nucleic Acids Res. 2015;43(15):e97. https://doi.org/10.1093/nar/gkv412.
75. Zhou Y, Zhou B, Pache L, et al. Metascape provides a biologist-oriented resource for the analysis of systems-level datasets. Nat Commun. 2019;10(1):1523. https://doi.org/10.1038/s41467-019-09234-6.
76. Shannon P, Markiel A, Ozier O, et al. Cytoscape: a software environment for integrated models of biomolecular interaction networks. Genome Res. 2003;13(11):2498–504. https://doi.org/10.1101/gr.1239303.

Publisher's note